J Seismol (2021) 25:351–367
https://doi.org/10.1007/s10950-020-09976-7

ORIGINAL ARTICLE

Seismicity in the Northern Rhine Area (1995–2018)

Klaus-G. Hinzen · Sharon K. Reamer · Claus Fleischer

Received: 24 August 2020 / Accepted: 2 December 2020 / Published online: 16 December 2020

Abstract Since the mid-1990s, the local seismic network of the University of Cologne has produced digital seismograms. The data all underwent a daily routine processing. For this study, we re-processed data of almost a quarter century of seismicity in the Northern Rhine Area (NRA), including the Lower Rhine Embayment (LRE) and the Eifel Mountain region (EMR). This effort included refined discrimination between tectonic earthquakes, mine-induced events, and quarry blasts. While routine processing comprised the determination of local magnitude M_L, in the course of this study, source spectra-based estimates for moment magnitude M_W for 1332 earthquakes were calculated. The resulting relation between M_L and M_W agrees well with the theory of an $M_L \propto 1.5\ M_W$ dependency at magnitudes below 3. By applying Gutenberg-Richter relation, the *b*-value for M_L was less (0.82) than M_W (1.03). Fault plane solutions for 66 earthquakes confirm the previously published N118° E direction of maximum horizontal stress in the NRA. Comparison of the seismicity with recently published Global Positioning System–based deformation data of the crust shows that the largest seismic activity during the observation period in the LRE occurred in the region with the highest dilatation rates. The stress directions agree well with the trend of major faults, and declining seismicity from south to north correlates with decreasing strain rates. In the EMR, earthquakes concentrate at the fringes of the area with corresponding the largest uplift.

Keywords Northern Rhine Area · Lower Rhine Embayment · Eifel · Seismicity · Moment magnitude · Crustal deformation

K.-G. Hinzen (✉) · S. K. Reamer · C. Fleischer
Department of Geosciences, University of Cologne, Cologne, Germany
e-mail: hinzen@uni-koeln.de

1 Introduction

The Northern Rhine Area (NRA) mainly comprises the region between the rivers Mosel, Rhine, and Maas (Fig. 1). Observation of its moderate seismicity started around 1905 with a station in the city of Aachen (Haußmann 1907). However, the main purpose of this station was to discriminate between natural tectonic earthquakes and mine tremors as the mine owners wanted to avoid reimbursements for damages caused by natural earthquakes (Hinzen 2011). In 1906 Haußmann, a mine surveyor and professor at the Technical University in Aachen, ordered a 1.3-ton Wiechert seismometer from the Spindler and Heuer company in Göttingen. Because he could not go himself, he sent his assistant Ludger Mintrop to Emil Wiechert, the first professor of geophysics at the Göttingen University, to receive instructions for maintaining the seismometer. Consequently, the interests of Mintrop, now regarded as the "father of exploration seismology," shifted from surveying to seismology (Haußmann 1907). The original station located in one of the mines was moved to a surface location because of trouble with high subsurface humidity that affected the recording paper. In 1908,

Mintrop (1909a, 1909b) moved to Bochum and installed a second seismic station. These two remained the only local stations operating until sometime during WW2. After the war, the Euskirchen earthquake of 1951 (Berg 1953), of magnitude 5.7 with damage of intensity VIII, triggered the interest of Martin Schwarzbach. At that time, Schwarzbach was director of the Geological Institute of the Universität zu Köln. He was eventually well known for his pioneering work on geology and climate (Schwarzbach 1963) but had no background as a seismologist. After applying for help from Wilhelm Hiller from Stuttgart, Schwarzbach established a local station in Bensberg (BNS), located 12 km east of the center of Cologne the station rested on Devonian hard rock (Fig. 1). This provided a more favorable place for seismic recording than the university campus near downtown Cologne on the eastern rim of the LRE above 360 m of Tertiary and Quaternary sediments (Ahorner 2008). Ludwig Ahorner expanded the one station enterprise into a network in the 1970s, referred to as BENS network. Between 1995 and 2000, all BENS network stations were converted to digital recording, and in 2006, the number of permanent stations reached 43 with 20 accelerometer stations.

Several scientific projects in the past explored different aspects of seismology in the NRA between Rhine, Maas, and Mosel for which data from permanent seismic stations produced a valuable database. From 1976 to 1982, the "Plateau Uplift" project employed an interdisciplinary approach to better understand the vertical movements of the Rhenish Shield still in the era before Global Positioning System (GPS) was available (Fuchs et al. 1983; Ahorner 1983). In the frame of the DECORP project in the 1980s, deep sounding seismic reflection profiles were measured throughout the Rhenish Massif (Meissner and Bortfeld 1990; DECORP 1991), the results improving the understanding of crustal structure and distribution of seismic velocities. The PALEOSIS project (Camelbeeck and Meghraoui 1996; Camelbeeck et al. 2001) revealed evidence for the first time of strong surface rupturing earthquakes during the Holocene in the LRE. The Eifel Plume Project, a large seismic tomography survey in 1997/1998, covered an area of approximately 400×250 km^2 centered on the Eifel volcanic fields with more than 200 permanent and temporary stations (Ritter et al. 2001). Results from the study strengthened the hypothesis of the existence of a mantle plume below the Eifel. Previously, in a tomographic study down to 70 km, Braun and Berckhemer (1993) had found an upper crustal low-velocity body under the Vogelsberg volcano. As part of the AGRIP-PINA project, array techniques to use ambient noise for the exploration of soft sediments were advanced with data measured in the LRE (Scherbaum et al. 2003).

Reamer and Hinzen (2004) transferred about 96,000 hand-written phase readings of earthquakes recorded between 1975 and 1995 with the BENS network into digital format and used the database to construct an optimized 1D velocity model and calibrate parameters for M_L determination. Beginning in 1999, the routinely processed data of the BENS network were reported online (http://www.seismo.uni-koeln.de, last accessed August 2020); through this link, the actual earthquake catalog is accessible.

In this paper, we report on the reprocessing of earthquakes recorded between 1995 and 2018, which comprise all events of the BENS network for which digital seismograms are available until the end of the observation period. The reprocessing of earthquakes in the study area (50° to 52° N and 6.5° to 8.5° E) included (1) control and if necessary re-picking of phases, (2) relocation, (3) re-discrimination of blasts and mine tremors falsely registered as tectonic earthquakes, and (4) for the first time the determination of moment magnitude M_W for all earthquake records where the signal-to-noise ratio (SNR) was sufficiently high providing the data necessary to (5) update the magnitude frequency relation for the study area. (6) Fault plane solutions were determined for events with more than ten unambiguous polarity readings. (7) The seismicity results are then further discussed with respect to GPS-based data of crustal deformation which recently became available through work by Kreemer et al. (2020).

2 The network

At the beginning of the observation period (1995), the BENS network consisted of seven short-period analog (FM tape) or semi-digital (PCM tape) recording stations. With the exception of one station (JUL) on the sediments in the LRE and inside the compound of an experimental nuclear facility, all other stations were located on the Rhenish Shield (Fig. 1). As noted, after 1995, all stations were converted to digital recording with AD converters originally designed by the Royal Observatory of Belgium (Snissaert 1992). Subsequent years saw the addition of several new short-period stations and one

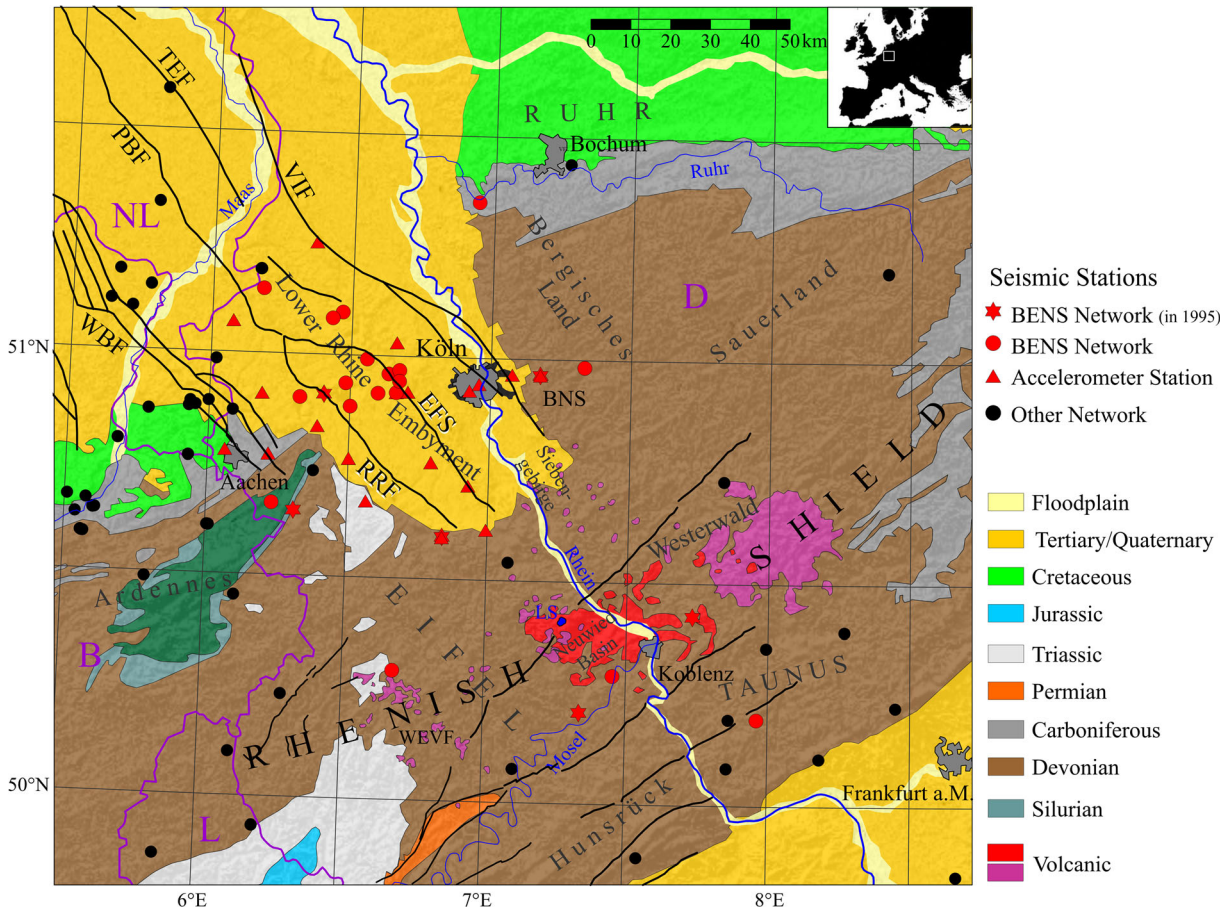

Fig. 1 Location of seismic stations in the Northern Rhine Area used in this study. Red symbols indicate stations of the BENS network of the University of Cologne. The stations from networks of other operators (black circles) were often used for the location of earthquakes. The white rectangle in the insert in the upper right corner indicates the location of the study area within Western Europe. The underlying terrain model is based on SRTM data (Farr et al. 2007) and the simplified geologic information is based on the 1:200,000 geologic map of Germany (Zitzmann 2003) and the Geologische Übersichtskarte Rheinland Pfalz (2020). Black lines show major faults: TEF Tegelen Fault, VIF Viersen Fault, PBF Pell Boundary Fault, WBF Western Border Faults, RRF Rurrand Fault, EFS Erft Fault System, LS Laacher See caldera; purple lines are national borders: B Belgium, D Germany, L Luxemburg, NL The Netherlands; WEVF West Eifel volcanic field; some cities and territories are indicated. The original station of the network east of Cologne is labeled with the station code BNS

broadband station (DREG). In 2001, a dozen stations equipped with short-period sensors for surveying the open lignite pit mines west of Cologne were integrated into the BENS network. The location of these "mining" stations changed from time to time, due to the advancing work face of the mines. In 2001, the recording hardware was updated to commercial 24-bit AD converters and industry-standard PCs with continuous recording in Nordic format (Havskov et al. 2020) which is still the status of the stations monitoring at the time of this contribution. This format was chosen for the acquisition software, because all routine processing was done by the SeisAn software package (http://seis.geus.net/software/seisan/, last accessed July 2020). Seismic event timing is controlled by DCF77 clocks. The network reached its current size of 43 stations in 2006 when 20 accelerometer stations were added (Hinzen and Fleischer 2007). Most of these strong-motion stations are in the free field placed on the soft sediments of the LRE, with changing sediment thicknesses from a few decameter to 1.3 km and in close vicinity to the active faults. These stations provided good records of events with magnitudes down to M_L 1 or even lower in case of small hypocentral distances. Four accelerometer stations

have been in use since 2010 to monitor the seismic response of Cologne Cathedral (Hinzen et al. 2012; Hinzen 2014).

The increase of the number of active stations after 2006 to 43 reduced the median inter-station distance within the network from 66 km (in 1995) to 44 km. Station locations and parameters are available at http://www.seismo.uni-koeln.de/station/netz.htm (last accessed July 2020). In addition to the BENS network (University of Cologne 2016), data from stations of neighboring networks are shown in Fig. 1. These include the Royal Observatory of Belgium (ORB) (Belgium 1985), the Koninklijk Nederlands Meteorologisch Instituut (KNMI 1993), Ruhr-Universität Bochum (RUB Germany 2007), Federal Institute for Geosciences and Natural Resources (GRSN 1976), Erdbebendienst Südwest (LED and LER), and the Geologischer Dienst NRW (GD NRW). Data from these stations were regularly utilized to locate earthquakes; however, magnitudes in the following are based only on seismograms from the BENS network. Since 2003, regular meetings twice a year with colleagues from ORB and KNMI helped to coordinate and improve cross-border seismic activities in the Rhine-Maas area and thereby continuing the initiative of an EU project "Rapid Transfrontier Seismic Data Exchange Network" which was coordinated by the British Geological Survey between 1994 and 1997.

3 Reprocessing

Data reprocessing included visual inspection of all phase picks, control and eventually re-picking of arrivals with unusual residuals, re-evaluation of event type (tectonic earthquake, mine-induced, explosion), re-localization, determination of M_L, and (with sufficient SNR) determination of M_W from distance-corrected displacement spectra of P- and/or S-phases. M_W had only been previously determined for 39 selected earthquakes with magnitudes larger than 2 which occurred between 1975 and 2001 (Reamer and Hinzen 2004). The distance correction we used for the M_L determination in this study is the one for the NRA given by Reamer and Hinzen (2004):

$$M_L = \log(A) + 1.2214\log(R) + 0.00106R - 2.2307 \quad (1)$$

where A is half the peak to peak Wood Anderson maximum trace amplitude with an amplification of 2080, and R the hypocentral distance.

3.1 Statistics

The raw catalog contained 14,782 events of which 7778 were categorized as tectonic or mine-induced earthquakes within the study area between 50° N and 52° N and between 5.5° E and 8.5° E. After reprocessing, 3330 tectonic earthquakes remained in the list and M_W could be determined for 1332 of them. (For 16 earthquakes in 1995, no magnitude could be determined.) The numerous non-tectonic events include mine-induced events from the deep coal mines in the Ruhr district (e.g., Casten and Cete 1980; Hinzen 1982; Gibowicz et al. 1990; Bischoff et al. 2010), open-pit lignite mines west of Cologne (Ahorner and Schaefer 2002), and quarry blasts. Not all detected quarry blasts were included in the daily routine processing; only examples of special interest were analyzed, based on the subjective decision of the seismologist on duty. The number and the distribution of quarry blasts in the study area were examined by Hinzen and Pietsch (2000) who estimated at the time of the study about 21,000 blasts per year (80 per working day) were fired, roughly 200 times the number of tectonic earthquakes. The sheer volume posed a particular challenge for the discrimination in routine processing.

Figure 2 shows the number of earthquakes per year for the 24-year period starting in 1995. The effect of densification of the network with the lowering of the detection threshold between 1995 and 2006 is indicated by the increase of detected tectonic events from 30 to more than 100 per year. Since 2010, the yearly number is around 200 earthquakes, with the increase primarily due to smaller earthquakes with magnitudes below M_L 1.0 being detected. The high number of almost 500 earthquakes in 2011 is due to the aftershock sequence of the 14. February event near Nassau (Hinzen 2019).

Further statistics on earthquakes occurrence is shown in Fig. 3, which breaks down the number of events per hour of the day, the minute, and the weekday. Time is local time and takes into account daylight saving time change in March and October of each year.

3.2 Earthquake map

The relocated epicenters of the dataset are shown on the map in Fig. 4; a complete list is available in the

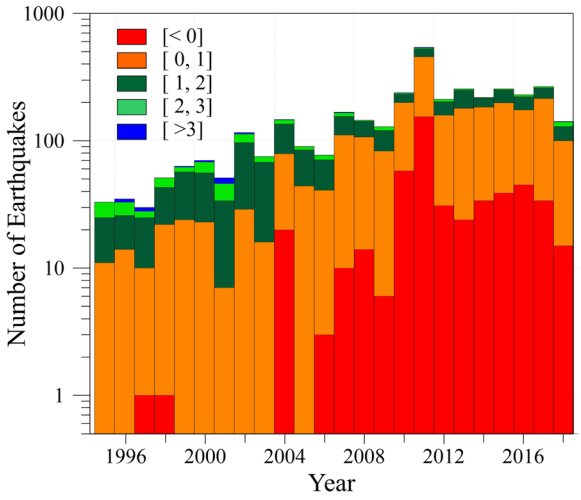

Fig. 2 Distribution of the number of earthquakes per year from 1995 to 2018. Colors of the stacked bars indicate the magnitude range given in the legend

Online Resource 1. Seismicity is concentrated in a NW-SE trending stripe which follows the direction of the maximum horizontal shear stress (N118° E) as was determined earlier from fault plane solutions (Hinzen 2003).

Seismicity north of the Neuwied Basin in the Ahr Area and the Siebengebirge (Fig. 1) forms a ~20-km-wide stripe trending parallel to the Rhine River valley with a sharp drop of activity towards NE and SW. On the right side of the river the activity extends north up to 50.9° N. Further north of this latitude, there are only two earthquakes in the dataset east of the Rhine River. Both occurred in 2015 within 20 min with magnitudes of M_L 1.9 and 1.6 at depths of 2–3 km. There were hints from the public who submitted macroseismic questionnaires that these events might have been associated with drilling activities in the area; however, this could not be confirmed.

The main seismic activity in the LRE is located in the western part with two stripes parallel to the Erft Fault System and the Rurrand Fault. The activity continues further north in the Netherlands where the fault is designated as Peel Boundary Fault the location of the 1992 Roermond earthquake (M_L 6) where seismic activity continued during the observation period.

The highest concentration of microearthquakes was observed in the Neuwied Basin south of the Laacher See volcano (compare Fig. 1). As stated in Section 4, these events include tectonic earthquakes as well as earthquakes, some with hypocenters below the crust, which can be associated with ongoing volcanic activity in the East Eifel volcanic field (Hensch et al. 2019).

For earthquakes with ten or more clearly identifiable polarity readings, fault plane solutions were made with a grid search. For 66 events, well-determined solutions were found and are listed in Online Resource 1; the mechanism for 27 of these with $M_L \geq 2.5$ are shown in Fig. 4.

3.3 M_L/M_W relation

The use of a consistent magnitude scale is essential in many sectors of seismological research. The moment

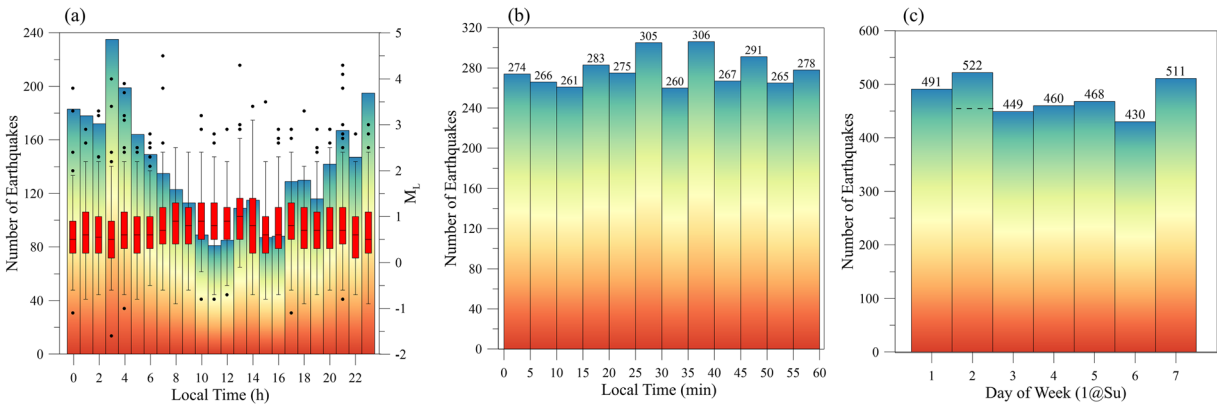

Fig. 3 Three histograms show the distribution of all relocated earthquakes with time. **a** Number of event per hour. Time is Central European Time (including daylight saving). The overlaid boxplots show the distribution of magnitudes (rightmost scale) per hour of the day. Red boxes show the 25 to 75% quartiles with a black line indicating the median; whiskers give 1.5 of the quartile range and black dots show outliers. **b** Number of earthquakes per minute after the hour in bins of 5 min. **c** Number of earthquakes sorted by weekday ("1" represents Sunday). The dashed line indicates the value for Monday without the aftershock sequence of the 2011 Nassau earthquake

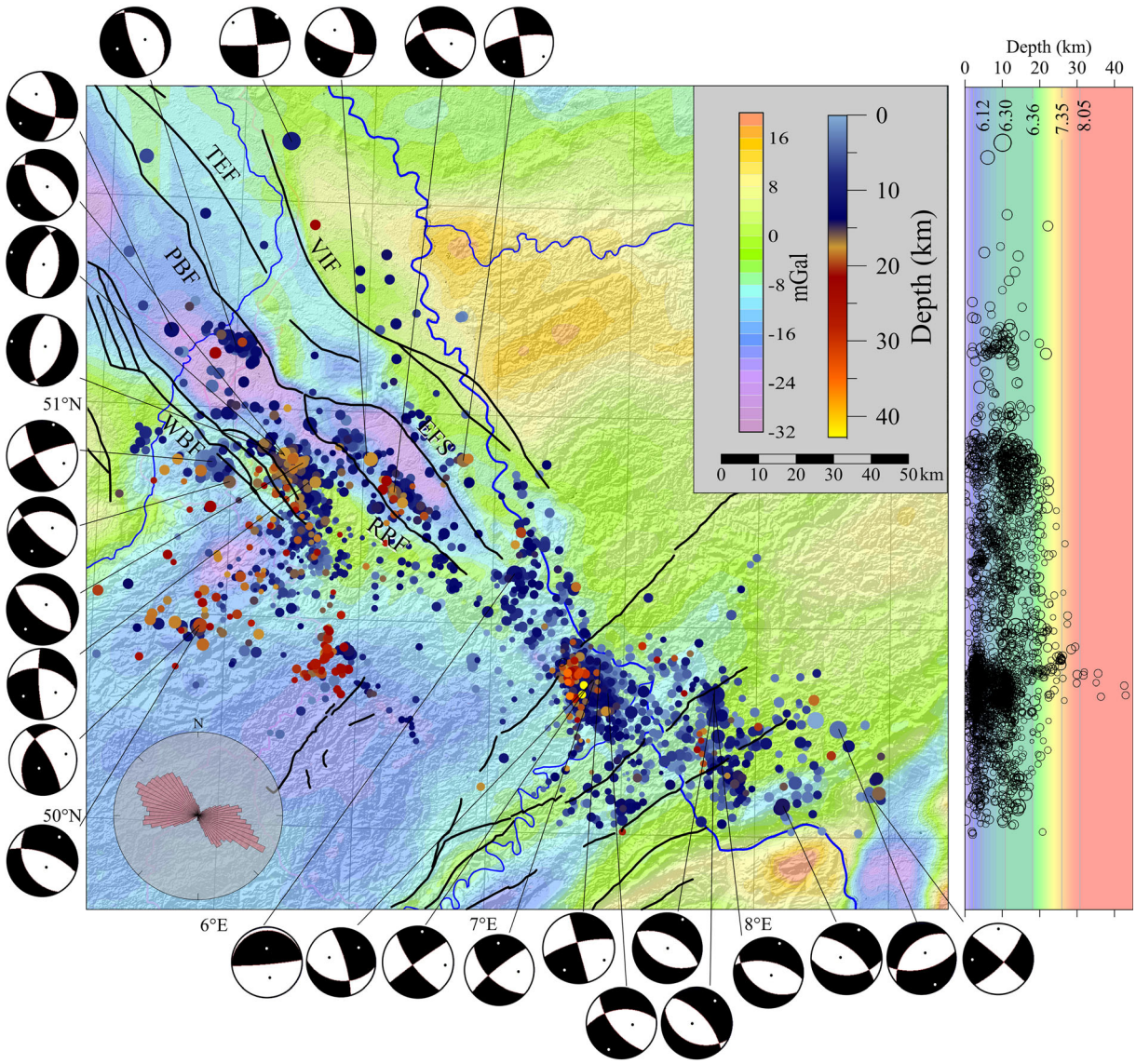

Fig. 4 Map of the Northern Rhine Area with the 3332 epicenters of the relocated earthquakes between 1995 and 2018, the color of the symbols indicates the depth of the hypocenter as shown in the legend. The color shade of the map shows the Bouguer gravity following the scale given in the legend (based on data from LIAG 2020). Black lines show major active faults in the Lower Rhine Embayment. The rose diagram inserted on the lower-left corner shows the direction of the greatest horizontal stress deduced from fault plane solutions (after Hinzen 2003). The graph on the right-hand side of the map shows the depth distribution of the earthquakes along a north-south profile, background color indicates the P-wave velocity of the 1D model (Reamer and Hinzen 2004), and numbers below the scale give the P-wave velocity in kilometers per second at major discontinuities. Focal mechanisms are shown for 27 earthquakes with $M_L \geq 2.5$. Thin black lines link the focal spheres to the epicenters on the map. Black and white dots indicate the P and T axes, respectively. TEF Tegelen Fault, VIF Viersen Fault, PBF Pell Boundary Fault, WBF Western Border Faults, RRF Rurrand Fault, EFS Erft Fault System

magnitude (Hanks and Kanamori 1979) has become a standard in the past decades. However, many (local) seismic networks, including BENS, do not determine M_W on a routine basis as M_L determination proves adequate particularly for earthquakes with magnitudes below 5. But particularly in regions with low to moderate seismicity and scarce earthquakes of magnitude 5 and above, the lower end of the magnitude frequency relation is important for determination of seismic hazard. Because many empirical relations between ground

motion and magnitude are now based on M_W, a reliable relation between M_L and M_W is essential when such ground motion models are applied. In the same way, as the distance calibration functions for M_L have to be determined individually for every region (Hutton and Boore 1987), there is no universal M_L/M_W relation that can be applied for all networks (Deichmann 2017).

We used spectral analysis of P- and S-wave phases to determine source parameters, including seismic moment, corner frequency of the source spectrum, and the related moment magnitude. Model spectra following Brune (1970) were fitted to distance-corrected displacement spectra using the SeiSan (Havskov et al. 2020) spectral modeling tool for all traces with sufficient SNR. The main processing steps are (1) removal of DC offset, (2) application of a cos-taper with 10% of the signal length at both ends, (3) FFT, (4) restitution of the instrument response, and (5) correction for attenuation along the travel path assuming a Q_0 of 540 (Romanowicz and Mitchell 2007). To fit the model spectra to the observed data, a frequency band with suitable SNR is selected by comparison to a time window of equal length prior to the first arrival, and then a grid search of the low-frequency level of the spectrum and the corner frequency is used to find the best fit. The results of all fitting procedures were visually controlled. The vertical component was used to analyze P-phases and both horizontal components for the S-phase, if possible.

A total of 1332 M_W values was determined from 16,295 spectra. Figure 5 a shows the distribution of M_L/M_W data pairs in bins of 0.1 magnitude units. Most earthquakes for which M_W could be determined fall in the range between $0.5 < M_L < 2.5$; the counts for the bins in Fig. 5a range from 1 to 22. In part (b) of Fig. 5, the difference of M_W–M_L is shown with respect to M_L.

Both linear and quadratic relations have been used to parametrize empirical relations between M_L and M_W (e.g., Grünthal and Wahlström 2003; Grünthal et al. 2009; Allmann et al. 2010; Goertz-Allmann et al. 2011; Munafò et al. 2016; Deichmann 2017). For our dataset with $-0.7 \le M_L \le 4.6$, both types of relations fit the data equally well (Fig. 5b):

$$M_W = 0.691 M_L + 0.757 \quad [R^2 = 0.926] \tag{2}$$

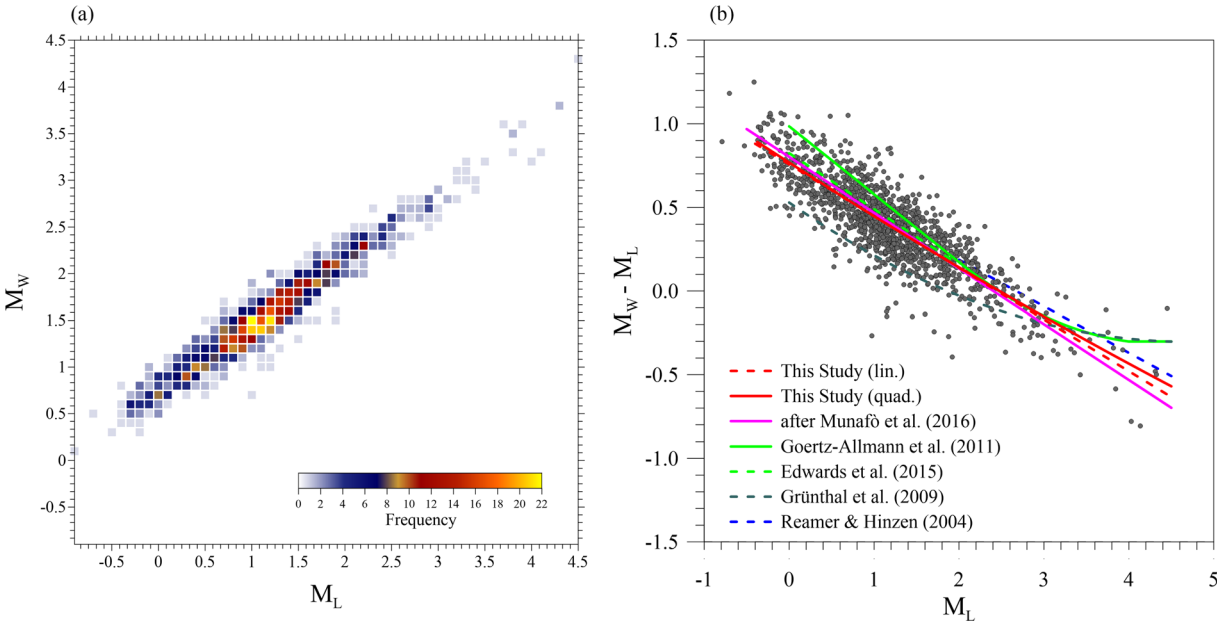

Fig. 5 **a** Moment magnitude with respect to local magnitude of the 1332 earthquakes for which M_W was determined in bins of 0.1 magnitude units. The color indicates the number of events in each bin. **b** The difference between moment magnitude and local magnitude for 1332 earthquakes of the Northern Rhine Area is shown by gray dots with respect to the moment magnitude. The solid and dashed red lines give the quadratic and linear best fits to the data in a least-squares sense, respectively. The magenta line follows the Munafò et al. (2016) concept of a 2/3 relation between M_W and M_L, with a constant of 0.80 for the best fit to the data. The continuous and dashed green lines are relations by Goertz-Allmann et al. (2011) with the addition of Edwards et al. (2015), respectively, for earthquakes in Switzerland, and the dark green line by Grünthal et al. (2009) for Central Europe. The dashed blue line gives the relation determined by Reamer and Hinzen (2004) for earthquakes in the Northern Rhine Area. All relations are shown within the magnitude range for which they were determined

$$M_W = 0.674M_L + 0.0064M_L^2 + 0.766 \quad [R^2 = 0.926] \tag{3}$$

3.4 Gutenberg-Richter model

Figure 6 shows two diagrams with the Gutenberg-Richter relation (Gutenberg and Richter 1956) of the cumulative frequency of earthquakes $\log N = a + bm$ in the study area for magnitude $m = M_L$ and $m = M_W$. The b-values differ for both relations: for M_L in the range from 1.0 to 4.5, $b = 0.82$ and for M_W between 1.5 and 4.3, $b = 1.03$.

4 Discussion

Even though the routine processing of the data from the BENS network has been competently performed over the years, the reprocessing has shown that overall data quality could still be improved.

The occurrence time statistic from Fig. 3 can indicate whether a significant number of man-made events remains in the catalog. In contrast to naturally occurring tectonic earthquakes, man-made events are not uniformly distributed in time. In particular, quarry blasts are bound to working days (Monday to Friday) and are often fired at specific and regular times often around midday and at the full hour (Hinzen and Pietsch 2000). Contamination with falsely classified quarry blasts would show skew in the histograms in Fig. 3. The clear trend of the histogram with 170 earthquakes per hour at night times and less than 100 earthquakes in the middle of the day is the reverse trend of the daily noise level. In the densely populated and highly industrialized study area (with an extensive highway and train network), there is a significant shift in the noise level affecting the frequency range of local earthquakes between 0.5 and 20 Hz; thus, the detection threshold increases from night to daytime, indicated by the boxplots of the magnitude distribution per hour overlaid in Fig. 3a. From 10 to 12 and 15 to 16 h local time, the average number of events per hour is 82. At 13 and 14 h, the number is increased to 109 and 115, respectively. This excess of about 50 events in 2 h might at first be seen as a sign of misclassified blasts. However, the M_L 4.3 Nassau earthquake on 14 February 2011(Hinzen 2019) had a strong aftershock sequence and 40 of these occurred between 13 and 15 h local time. Furthermore, the number of events per minute does not indicate larger values around the full hour as it would be the case with more blasts.

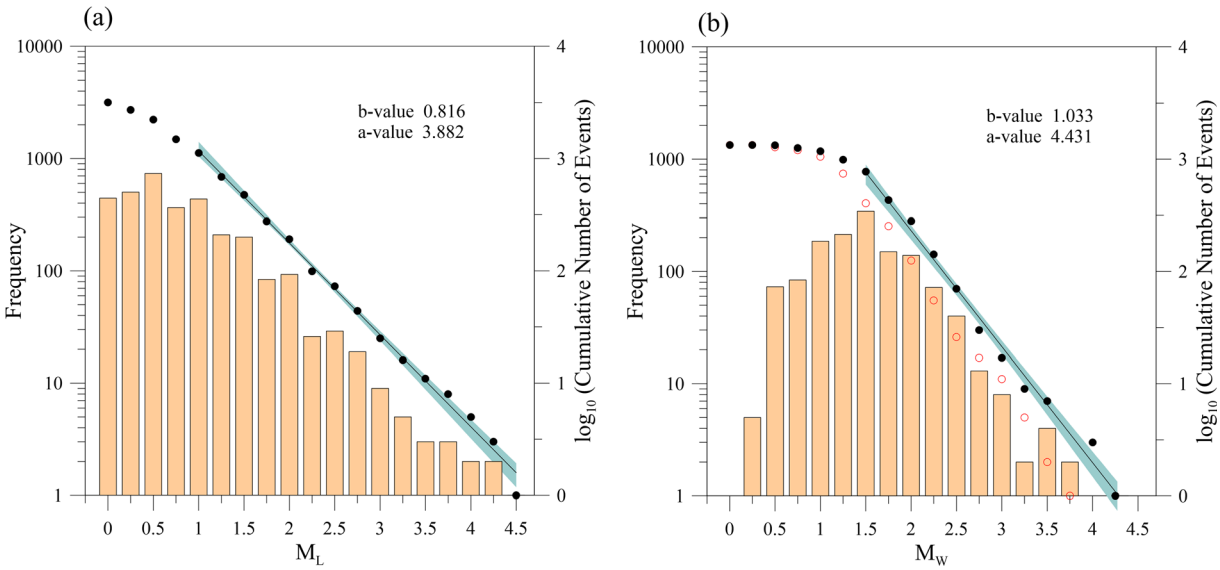

Fig. 6 **a** Histogram of magnitude frequency for the 3314 relocated earthquakes and the cumulative number (black dots) of earthquakes with the Gutenberg-Richter relation for the magnitude range $1 < M_L < 4.5$. The a- and b-values are given in the top right corner and the 95% confidence range of the fit is indicated in light blue. **b** Same as in **a** for the 1332 earthquakes for which M_W was determined with the Gutenberg-Richter relation for $1.5 \leq M_W \leq 4.3$. The red circles give the corresponding M_W values converted from M_L using Eq. (8)

The largest number per day of the week was observed on Mondays with 511, but again 67 of these were aftershocks of the 2011 Nassau earthquake. Neglecting these aftershocks, the average number on a work day is 452 ± 14. The somewhat higher number of events on Sundays (491) and Saturdays (511) can be attributed to the lower noise levels on weekends.

In Fig. 5, the relation between M_L and M_W for the NRA is compared to results of previous studies. The slightly different slope of the linear relation of 0.691 compared to the 0.722 derived by Reamer and Hinzen (2004) for the same region can be attributed to the different covered magnitude ranges. Reamer and Hinzen (2004) used 39 events with magnitudes M_L above 2.0. For most of those, only a limited number of phases could be used due to the few digital seismograms available from the study time period 1975 to 2001 compared to 1332 events for this study with many more digital seismograms available.

Grünthal et al. (2009) updated the work by Grünthal and Wahlström (2003) and proposed a M_L/M_W relation for Central Europe based on 221 data pairs with original M_W determinations mostly from the Swiss moment tensor solutions (Fäh et al. 2011):

$$M_W = 0.53 + 0.646M_L + 0.041\,M_L^2 \quad (4)$$

The data set on which Eq. (4) is based mainly contained earthquakes with M_W above 2 and up to 6, only six events had magnitudes below 1. As shown in Fig. 5b, this relation for Central Europe somewhat underestimates M_W for the small earthquakes in the Northern Rhine Area; at $M_L = 1.0$ for example, the linear fit to our data in Eq. (2) predicts $M_W = 1.45$, while with Eq. (4), it is $M_W = 1.22$.

Goertz-Allmann et al. (2011) used earthquakes in Switzerland recorded between 1998 and 2009 to estimate a M_L/M_W relation in the magnitude range $0.0 \leq M_L \leq 5.4$ with three different functions:

$$\begin{gathered} M_W = 0.594M_L + 0.985 \quad [0 \leq M_L \leq 2.0] \\ M_W = 1.327 + 0.253M_L + 0.085M_L^2 \quad [2.0 < M_L \leq 4.0] \\ M_W = M_L - 0.3 \quad [4.0 < M_L] \end{gathered} \quad (5)$$

This relation agrees with our linear fit (2) at M_L 2, but Eq. (5) predicts slightly larger values at low magnitudes with $M_W = 1.58$ compared to 1.45 at $M_L = 1.0$.

By referring to the stochastic waveform models of Hanks and Boore (1984), Edwards et al. (2015) proposed to change the slope in relation (5) at M_L smaller than 2 to a value of 2/3 (0.667) instead of 0.594 (Deichmann 2017):

$$M_W = 0.667M_L + 0.824 \quad [0 \leq M_L \leq 2.0] \quad (6)$$

In a recent paper, Munafò et al. (2016) by applying random vibration theory showed that for small earthquakes with a M_W below 4, M_L is proportional to the logarithm of the seismic moment and the corresponding relationship between the magnitudes is:

$$M_W = \frac{2}{3}M_L + C' \quad (7)$$

where C' is a free constant individual to the region and data set. In a test with a data set from the Upper Tiber Valley (northern Apennines, Italy) of 1191 earthquakes, they determined a C' of 1.15. Assuming a fixed slope of 2/3 for our data set of 1332 events in the NRA, the best fit for C' is 0.802 (Fig. 5):

$$M_W = 0.667M_L + 0.802 \quad [-1.0 \leq M_L \leq 4.3] \quad (8)$$

and predicts $M_W = 1.47$ at $M_L = 1.0$ compared to 1.45 with relations (2) and (3).

Deichmann (2017) did a detailed study using model calculations and empirical analysis and concluded by referring to Hanks and Boore (1984), Edwards et al. (2010, Edwards et al. 2015), and Munafò et al. (2016) that in an attenuating medium for small earthquakes below some magnitude threshold, the 2/3 slope to be almost unrefutable. The question of what the magnitude threshold is below which the 2/3 slope applies is not easy to answer. Deichmann (2017) found a gradual transition even in a rather homogeneous dataset of induced events from a limited source volume, all recorded at the same borehole station, and concluded the magnitude threshold is clearly a function of the degree of attenuation along the travel path. For a dataset like ours which averages the M_L/M_W relation over a comparatively large area of epicenters and uses data from some 40 stations, Deichmann (2017) places the threshold somewhere between M_W 2 and 4, depending on the attenuation conditions. As our dataset contains only 21 events with M_L above 3.0 but 929 with M_L between 0.5 and 2.0, an unambiguous threshold cannot be stated; however, below M_L 3.0, the application of Eq. (8) seems to be justified.

These differences between M_L and M_W for low magnitudes also affect the corresponding Gutenberg-Richter

relations. For our dataset, the *b*-value for the M_L relation (0.82) is lower than for the M_W relation (1.03). Deichmann (2017) reported a similar trend for the earthquakes of the Swiss earthquake catalog, with a lower *b*-value for M_L compared to M_W; however, in that study, the M_W values were converted from M_L using the relation by Goertz-Allmann et al. (2011) with the modification by Edwards et al. (2015) (Eqs. (5) and (6)). For BENS values of M_W were directly determined from the seismic records, Fig. 5b shows in addition to the directly determined M_W values (black dots), the values which result when the measured M_L data are converted to M_W using Eq. (8) (red circles). Below $M_W = 2.5$, the *b*-value of the converted data (1.02) is similar to the one obtained from measured data (1.03), but due to the influence of the few stronger earthquakes, a change in the *b*-value of the converted data to 1.11 occurs at magnitudes above 2.5. The largest measured M_W is 4.3, but the corresponding converted value only 3.8.

As an additional check on the clustering of hypocenters, the double-difference (DD) method (Waldhauser 2001) was applied to the dataset of 51,209 differential arrival times. Limiting the search for clusters to events with a minimum of four links resulted in 824 hypocenters in 18 clusters. Figure 7 shows these earthquakes together with the rest of the dataset and the frequency depth distribution of the earthquakes in nine selected areas.

The three areas within the LRE, entitled Erft, Rur, and Roermond, contain about 25% of all earthquakes in the database. Most events in the Erft cluster occurred at depths between 6 and 15 km with a maximum depth of 26 km. The epicenters align in a pattern parallel to the Erft Fault System (Fig. 7) at a horizontal distance indicating a westward dip of the faults of about 50 to 55°. In the Rur cluster, more earthquakes are located at a shallower depth between 4 and 14 km. A clear association with one of the faults in the Rur area is not easy because at depth they can occur on either the westward-dipping Rurrand Fault or on one of the east-dipping Western Border Faults. For example, the fault plane solution of the 2002 Alsdorf earthquake (M_W 4.3, depth 15.8 km) indicates a normal faulting mechanism on a 52° west-dipping plane which can be associated with the Rurrand Fault (Hinzen and Reamer 2007). The earthquakes in the Roermond cluster are in the vicinity of the strongest earthquake in the NRA in the past century with M_W 5.4 (Camelbeeck et al. 1994) and linked to the Peel Boundary Fault (Fig. 7).

The Voerendaal cluster in the Dutch province of Limburg shows a large percentage (46%) of hypocenters at shallow depth between 2 and 6 km. These earthquakes were part of small swarms of events between 2000 and 2001 (Dost et al. 2004). The proximity to former coal mines suggests the possibility that these shallow events may be associated in a causal sense due to the rising water table after the abandonment of these mines (Sigaran-Loria and Slob 2019) which produces heterogeneous surface displacements detected by satellite radar interferometry (Caro Cuenca et al. 2013).

The clusters in the Ardennes and in the West Eifel show hypocenters in the lower crust, almost reaching the Moho at 30 km. The high percentage of events with depth of 12 to 14 km in the West Eifel is due to two small swarms of microearthquakes in 2010 at this depth level.

More than 40% of all earthquakes are located within the Neuwied Basin cluster. While the majority of tectonic earthquakes in and around the basin has shallow hypocenters of less than 10 km, some events have been observed at depths reaching 40 km, well below the Moho discontinuity. Hensch et al. (2019), using data from temporary as well as permanent stations, showed that deep low-frequency microearthquakes below the Laacher See Volcano occurred in four distinct clusters between 10- and 40-km depth. The Laacher See is the caldera of the last eruption in the East Eifel volcanic field 12.9 Kyr ago, which was fed by a shallow magma chamber at 5- to 8-km depth, erupting a total magma volume of 6.7 km^3 (Zolitschka et al. 2000; Schmincke 2007, 2009).

In the Taunus, the majority of hypocenters occur at depths shallower than 15 km. Some of the events form lineaments in the SW-NE direction roughly parallel to faults in the Devonian bedrock. In the Ahr cluster, two bands of epicenters stretch NE-SW and NNE-SSW across the Rhine River. The northern part of these bands includes earthquakes in the Siebengebirge, where the last volcanic activity occurred in the Miocene, and north of it on the eastern side of the Rhine River. Hypocenters in this cluster are mainly shallow, around 2 to 5 km and between 10 and 14 km.

Of the 66 fault plane solutions from the earthquakes with more than 10 unambiguous polarity readings (Online Resource 1 and Fig. 4), 30% have strike-slip character, while the others mainly conform to a normal faulting mechanism. Application of the linear inversion algorithm from Michael (1984) reveals a trend of the

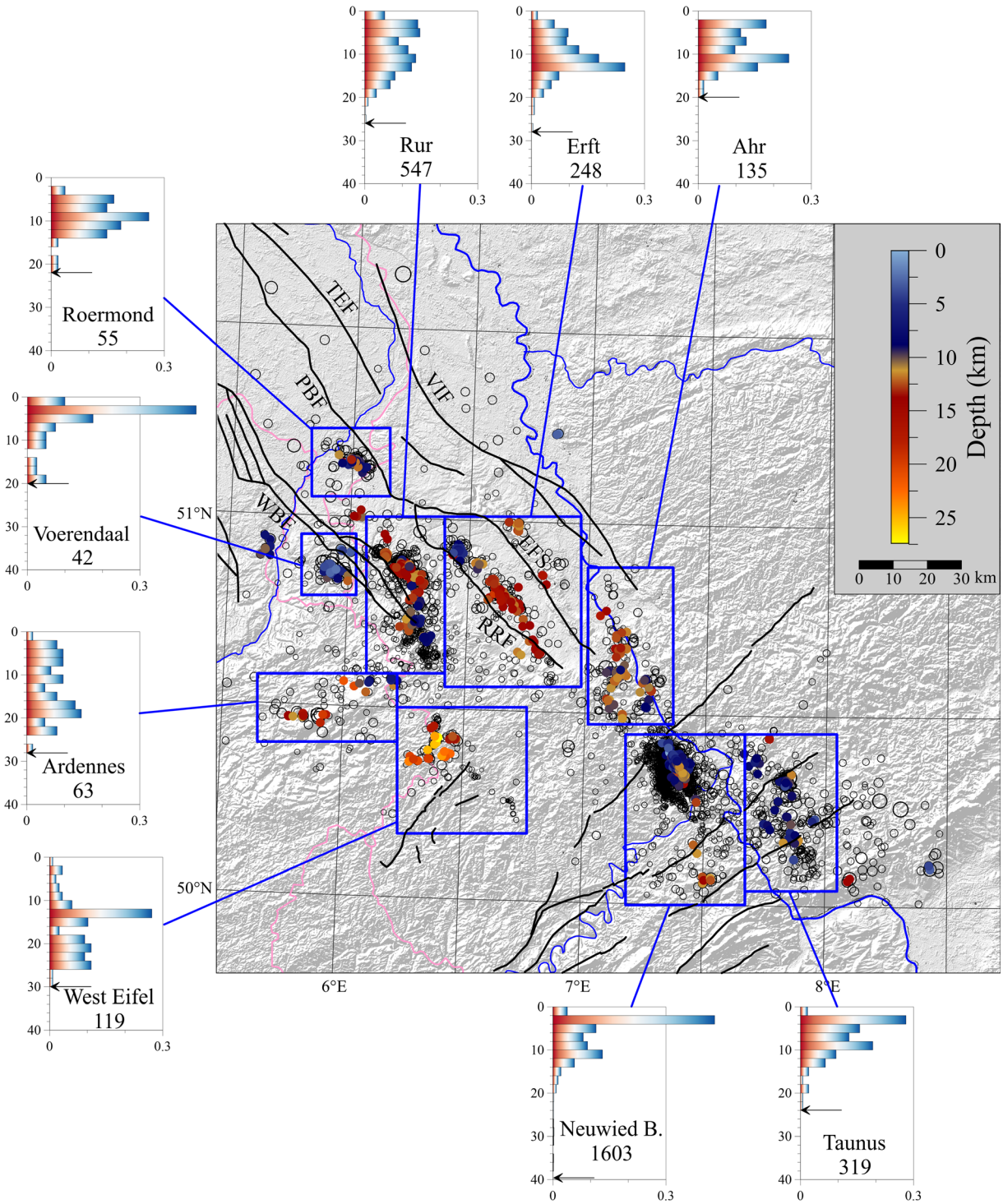

Fig. 7 Circles show the epicenters of the earthquakes (1995–2018). Colored dots mark earthquakes which were relocated with the double-difference method (Wadthauser 2001). Black lines are major faults. The blue rectangles indicate nine areas with earthquake clusters and the associated bar charts show the depth distribution of the hypocenters for each cluster. Below the name, the number of earthquakes in the rectangle is shown and arrows indicate the maximum observed depth. TEF Tegelen Fault, VIF Viersen Fault, PBF Pell Boundary Fault, WBF Western Border Faults, RRF Rurrand Fault, EFS Erft Fault System

largest compressive stress in the NRA of N118° E. This value is identical to the maximum horizontal stress direction determined by Hinzen (2003). (Also, see the rose diagram in Fig. 4; eight of the 66 fault plane solutions from this study were also part of the database used by Hinzen 2003).

In a recently published paper, Kreemer et al. (2020) used Global Positioning System (GPS) data to robustly image vertical land motion (VLM) and horizontal strain rates over most of intraplate Europe. They found a clear spatially coherent positive VLM anomaly over a large area surrounding the Eifel volcanic fields with maximum uplift of ~ 1 mm year^{-1} at the center (when corrected for glacial isostatic adjustment) and significant horizontal extension surrounded by a radial pattern of shortening. This combination strongly suggests a common dynamic cause (Kreemer et al. 2020). Their uplift model postulates a mantle plume at the bottom of the lithosphere. The location of the modeled plume agrees well with the findings by Ritter (2007) from the large-scale seismic experiment, the Eifel Plume project.

The deformation field deduced by Kreemer et al. (2020) is based on continuous GPS data of more than 2100 stations operating across Europe for up to ~20 years. The GPS station density in the central part of Europe in the Kreemer et al. (2020) dataset includes more than 70 stations within our study area (Fig. 8), sufficient to compare the deformations with seismicity recorded in the study area over the past quarter century.

The dataset from Kreemer et al. (2020) contains horizontal and vertical velocities and deformation resolved on a 0.1° grid. From these data, we calculated the maximum shear strain:

$$\dot{\varepsilon}_{\mathrm{maxshear}} = \frac{\lambda_1 - \lambda_2}{2} \tag{9}$$

where $\lambda_{1,\,2}$ are the eigenvalues of the strain rate tensor with components $\dot{\varepsilon}_{xx}$, $\dot{\varepsilon}_{yy}$, and $\dot{\varepsilon}_{xy}$ and the directions of maximum shear strain rate (Hackl et al. 2009):

$$\theta_{1,2} = \frac{1}{2}\arctan\left(\frac{2\dot{\varepsilon}_{xy}}{\dot{\varepsilon}_{xx} - \dot{\varepsilon}_{yy}}\right) \pm 45° \tag{10}$$

and the trace of the tensor corresponds to the relative variation rate of the surface area (dilatation) (Hackl et al. 2009):

$$\delta = \dot{\varepsilon}_{xx} + \dot{\varepsilon}_{yy} \tag{11}$$

Figure 8 shows the seismicity with respect to the vertical land movement corrected for the far-field glacial isostatic adjustment signal (Kreemer et al. 2020) and the

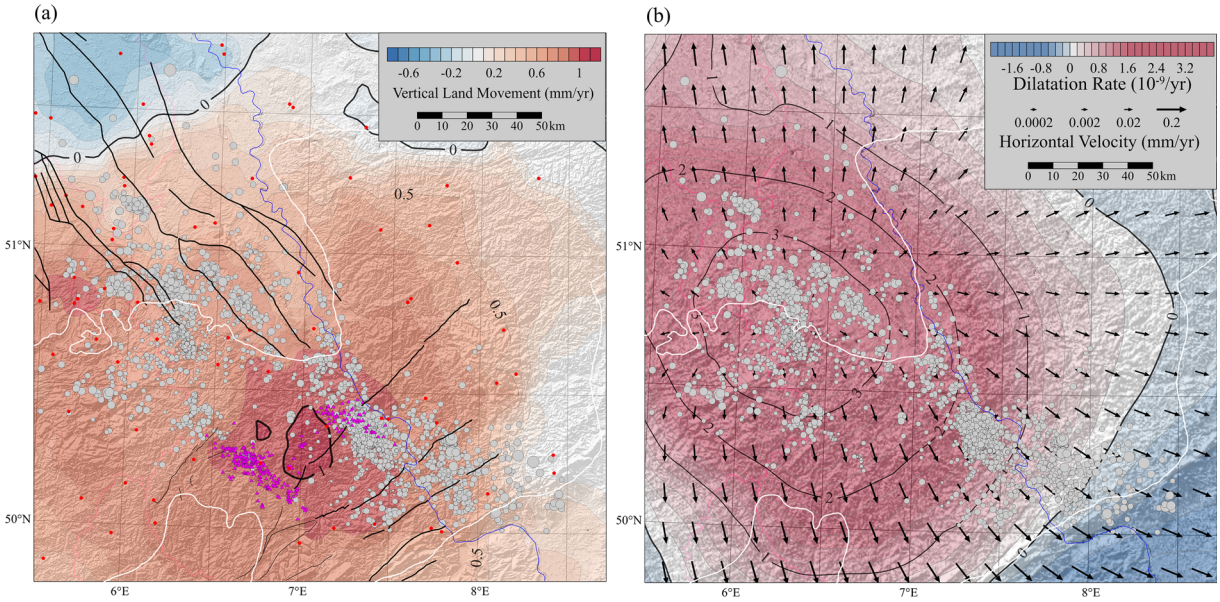

Fig. 8 **a** Gray circles are the epicenters of the 3314 relocated earthquakes in the Northern Rhine Area (1995–2018). Major faults are shown in black, and the edge of the Rhenish Shield is indicated by white lines. **a** The colored contours show the vertical land movement determined from GPS measurements by Kreemer et al. (2020) corrected for the far-field glacial isostatic adjustment signal. Triangles give the locations of volcanoes in the west and East Eifel volcanic fields (after Meyer 2013). **b** Same map area as in **a** with color-coded dilatation rates and vectors of horizontal velocities based on a model inferred from the GPS data by Kreemer et al. (2020)

dilatation rate after Eq. (11) with the overlain horizontal velocities. The vertical movements show a clear maximum slightly above 1 mm/year in the center of the Eifel between the west and East Eifel volcanic fields (Meyer 2013; Schmincke 2009). In the area of the largest vertical movements (around 1 mm/year) with its center at 50.3° N and 7.0° E, few earthquakes have been observed in the past 25 years. On the other hand, at the fringe of that area, where the gradients of vertical movement are large with respect to the center of the uplifted area, clusters of earthquakes exist (i.e., along the Rhine River valley and in the Neuwied Basin, in the Hunsrück, in the Ahr region extending to the Siebengebirge, and northwest of the West Eifel volcanic field). With the exception of a small swarm of earthquakes with magnitudes below 0.5 which occurred within a few days in 2010, few events were recorded in the West Eifel volcanic field.

The largest dilatation rates are found at the western border of the LRE with a maximum of 3.7 10^{-9}/year at 50.7° N and 6.4° E. As shown in Fig. 8b, horizontal velocities are practically zero at the center of the dilatation and increase with distance from it pointing radially away. In the range of the largest dilatation lies the Rur cluster of earthquakes (Fig. 7), which also includes the 2002 Alsdorf earthquake (M_W 4.3), (Hinzen 2005). In addition, increased seismicity was observed here in the two years following the 1992 M_W 5.4 Roermond earthquake (Camelbeeck et al. 1994) which occurred 40 km northwest of the Alsdorf event (Hinzen and Reamer 2007). A similar pattern of horizontal extension in this area was noted by Camelbeeck and van Eck (1994) based on an analysis of 24 fault plane solutions.

The maximum shear strain (Eq. 8) shown in Fig. 9a together with the seismicity reveals lowest shear strain values are found in the Eifel, south of the West Eifel volcanic field, and in the northern part of the LRE. The low shear strain in the Eifel may correlate with the low seismicity in this area. In addition to the shear strain values, two (indistinguishable) directions of the maximum shear (Eq. 9) are shown in Fig. 9a. In addition to the direction at the grid points of the map (gray symbols), the directions along the major faults in the LRE and along some lineaments of the seismicity pattern within the Rhenish shield are plotted (red symbols). The directions agree well with the trend of the faults;

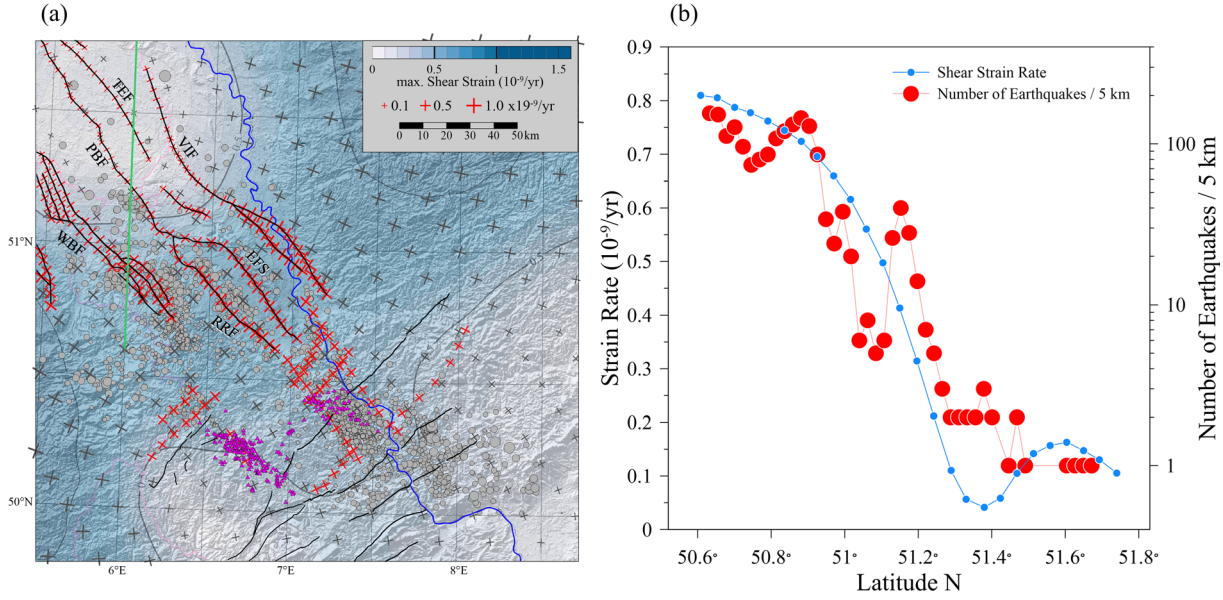

Fig. 9 **a** Color-coded maximum shear strain map based on a model inferred from the GPS data by Kreemer et al. (2020). The crosses give the direction of the maximum shear strain rate, with their size scaled to shear strain rate amplitude. Gray crosses are shown at every third grid point (for better visibility). The red crosses show the directions along the Quaternary faults of the Lower Rhine Embayment and along some lineaments in the southern part of the map. Gray circles show epicenters of earthquakes (1995–2018). TEF Tegelen Fault, VIF Viersen Fault, PBF Pell Boundary Fault, WBF Western Border Faults, RRF Rurrand Fault, EFS Erft Fault System. **b** The shear strain rate amplitudes are plotted with respect to latitude along a NS trending profile at 6° E starting at the southern tip of the LRE (indicated in the map by the green line). The red dots show the number of earthquakes in 5-km-wide horizontal stripes along the profile overlapping by half the bin width

e.g., they align even with the bends in the trend of the Viersen Fault and the Erft Fault system (Fig. 9a). The size of the symbols, scaled by the maximum shear strain, displays a clear decrease of this value from south to north in the LRE. To quantify this observation, in Fig. 9b, the strain rate is plotted along a south-north trending profile at 6° E (shown in Fig. 9a). In addition, Fig. 9b shows the number of earthquakes along this profile in 5-km-wide east-west trending stripes which overlap by half of the bin width from the southern end of the LRE to the northern limit of the study area. The decrease of earthquake frequency in the LRE from south to north correlates well with the decrease in shear strain rate.

The directions of shear are also found to be parallel to some lineaments in the seismicity pattern in the West Eifel, and the Middle Rhine Area. In particular, the NW-SE trend of the limits of seismicity agrees well with the NW-SE shear direction (Fig. 9a).

5 Conclusions

The reprocessing of almost a quarter century of digital seismic data from the BENS network resulted in an updated earthquake catalog. Direct determination of moment magnitudes of 1332 small earthquakes supports the hypothesis $M_L \propto 1.5\ M_W$ for magnitude below 3. An updated Gutentenberg-Richter relation with measured moment magnitudes ($1.5 \leq M_W \leq 4.3$) reveals higher *b*-value of 1.03 than a 0.83 *b*-value based on local magnitudes. Fault plane solutions confirm a maximum horizontal stress at N118° E. Comparing the seismicity with recently published GPS-based deformation data shows that most earthquakes in the Lower Rhine Embayment in the past two and a half decades occurred within an area corresponding to maximum crustal dilatation. The direction of shear strain agrees well with the trend of major normal faults of the LRE. The decrease in seismic activity from south to north correlates with the decrease in shear strain rate. In the Eifel Mountain Region, the area with largest uplift rates (reaching 1 mm/year) shows few earthquakes; however, at the fringes of this area where the gradient of vertical movement is large, numerous earthquakes occurred during the observation period. In the Middle Rhine Area, lineaments in the seismicity pattern are parallel to one of the maximum shear directions.

The Northern Rhine Area has low to moderate seismicity. The 25 years of earthquake data from the BENS network do not include any spectacular damaging earthquakes. This deceptively low level of seismic hazard has led public and authorities to repeatedly underestimate the earthquake risk in this densely populated and highly industrialized area. The damaging earthquakes of the past century and those known from the historical record signify the risk. A recurrence of one of the surface rupturing earthquakes as evidenced by paleoseismic studies would result in major destruction in the study area. Therefore, continued and even intensified surveillance of the seismic activity in the NRA is essential for mitigating earthquake risk in addition to monitoring the volcanic activity in the Eifel Region.

Supplementary Information The online version contains supplementary material available at https://doi.org/10.1007/s10950-020-09976-7.

Acknowledgments Over the past 25 years, many people supported the research carried out at the Seismological Station Bensberg of the University of Cologne that we cannot adequately thank all the individuals in the danger of forgetting someone. In general, we thank all students and staff of the Seismological Station Bensberg who were part of the team that produced the data for this study. The work would not have been possible without the help from many individuals and companies who supported the establishing and continuous operation of the seismic stations. We are grateful to the colleagues of our neighboring networks Observatoire Royal de Belgique, Koninklijk Nederlands Meteorologisch Instituut, German Regional Seismic Network, Ruhr-Universität Bochum, Erdbebendienst Südwest, and Geologischer Dienst NRW for the cooperation and data exchange and to the Dombauverwaltung of Cologne Cathedral. We also thank the administration of the University of Cologne, colleagues of the Institute of Geology and Mineralogy, and the Department of Geosciences who supported the work at the station in Bensberg. We thank C. Kreemer for providing the GPS-based deformation data and the fruitful discussion about them; we acknowledge the helpful comments by T. Camelbeeck on an early version of the manuscript and the input from P.B.A. Hinzen to calculate eigenvalues of deformation matrixes. We thank editor T. Braun for handling the manuscript and his comments in addition to two reviewers for constructive suggestions that improved the manuscript. Most of the data processing was made with the Seisan software package and we thank J. Havskov, P.H. Voss, and L. Ottemöller; figures were prepared with programs Grapher and Surfer of Golden Software.

Funding Open Access funding enabled and organized by Projekt DEAL. Funding was provided from the University of Cologne, *Freunde der Universität zu Köln*, the German Research Foundation (DFG), the *Dombauverwaltung* of Cologne Cathedral,

and RWE Power AG. Open access funding was provided by project DEAL.

Compliance with ethical standards

Conflict of interest The authors declare that they have no conflict of interest.

References

Ahorner L (1983) Historical seismicity and present-day micro-earthquake activity of the Rhenish Massif, Central Europe. In: Fuchs K, von Gehlen K, Mälzer M, Murawski H, Semmel A (eds) Plateau uplift. Springer, Berlin, pp 198–221

Ahorner L (2008) Geschichte der Erdebenstation Bensberg. Deutsche Geophysikalische Gesellschaft, http://dgg-online.de/geschichte/birett/BAND21.HTM. Accessed July 2020

Ahorner L, Schaefer W (2002) Induzierte Seismizitaet im Braunkohlengebiet der Niederrheinischen Bucht, Germany. Glückauf Forschungshefte 63:20–34

Allmann B, Edwards B, Bethmann F, Deichmann N (2010) Determination of M_W and calibration of M_L/M_W regression. Appendix A to ECOS 09 Earthquake Catalogue of Switzerland 2011 Report SED/RISK/R/ 001 20110417

Belgium ROO (1985) Belgian seismic network. International Federation of Digital Seismograph Networks. https://doi.org/10.7914/SN/BE

Berg H (1953) Das Rheinlandbeben bei Euskirchen vom 14. März 1951. Geofisica Pura e Applicata 24:57–67. https://doi.org/10.1007/BF01996049

Bischoff M, Cete A, Fritschen R, Meier T (2010) Coal mining induced seismicity in the Ruhr area, Germany. Pure Appl Geophys 167:63–75

Braun T, Berckhemer H (1993) Investigation of the lithosphere beneath the Vogelsberg volcanic complex with P-wave travel time residuals. Geol Rundsch 82:20–29. https://doi.org/10.1007/BF00563267

Brune JN (1970) Tectonic stress and the spectra of seismic shear waves from earthquakes. J Geophys Res 75:4997–5009

Camelbeeck T, Meghraoui M (1996) Large earthquakes in northern Europe more likely than once thought. Eos 405:409

Camelbeeck T, van Eck T (1994) The Roer Valley Graben earthquake of 13 April 1992 and its seismotectonic setting. Terra Nova 6:291–300

Camelbeeck T, vanEck T, Pelzing R, Ahorner L, Loohuis L, Haak HW, Hoang-Trong P, Hollnack D (1994) The 1992 Roermond earthquake, the Netherlands, and its aftershocks. Geol Mijnb 73:181–197

Camelbeeck T, van den Berg M, Meghraoui M, Galadini F (2001) Evaluation of the potential for large earthquakes in present-day low seismic activity regions of Europe. Netherlands Journal of Geosciences - Geologie en Mijnbouw 80:61–61. https://doi.org/10.1017/S0016774600022332

Caro Cuenca M, Hooper AJ, Hanssen RF (2013) Surface deformation induced by water influx in the abandoned coal mines in Limburg, The Netherlands observed by satellite radar interferometry. J Appl Geophys 88:1–11. https://doi.org/10.1016/j.jappgeo.2012.10.003

Casten U, Cete A (1980) Induzierte Seismizität im Bereich des Steinkohlenbergnaus des Ruhrreviers. Glückauf Forschungshefte 41:12–16

Deichmann N (2017) Theoretical basis for the observed break in M_L/M_W scaling between small and large earthquakes. Bulletin of the Seismological Society of America 107. https://doi.org/10.1785/0120160318

DEKORP Research Team (1991) Results of the DECORP 1 BELCORP-DEKORP deep seismic reflection studies in the western part of the Rhenish Massif. Geophys J Int 106:203–227

Dost B, vanEck T, Haak H (2004) Scaling of peak ground acceleration and peak ground velocity recorded in the Netherlands. Bollettino di Geophisica Theoretica ed Applicata 45:153–168

Edwards B, Kraft T, Cauzzi C, Kästli P, Wiemer S (2015) Seismic monitoring and analysis of deep geothermal projects in St. Gallen and Basel. Switzerland Geophys J Int 201:1020–1037. https://doi.org/10.1093/gji/ggv059

Fäh, D, Giardini D, Kästli P, Deichmann N, Gisler M, Schwarz-Zanetti G, Alvarez-Rubio S, Sellami S, Edwards S, Allmann B, et al (2011) ECOS-09 earthquake catalogue of Switzerland release 2011 report and database, public catalogue, 17/04/2011. Report SED/RISK/R/001/ 20110417, Swiss Seismological Service ETH Zurich

Farr TG, Rosen PA, Caro E, Crippen R, Duren R, Hensley S, Kobrick M, Paller M, Rodriguez E, Roth L, Seal D, Shaffer S, Shimada J, Umland J, Werner M, Oskin M, Burbank D, Alsdorf D (2007) The shuttle radar topography mission. Rev Geophys 45. https://doi.org/10.1029/2005RG000183

Fuchs K, Gehlen KV, Malzer H, Murawski H, Semmel A (1983) Plateau uplift: The Rhenish Shield – a case history. Springer-Verlag, Berlin and Heidelberg

Geologische Übersichtskarte von Rheinland Pfalz (2020) https://www.lgb-rlp.de/karten-und-produkte/online-karten/online-karte-guek-300.html. Accessed 02 July 2020

Gibowicz SJ, Harjes H-P, Schäfer M (1990) Source parameters of seismic events at Heinrich Robert mine, Ruhr basin, Federal Republic of Germany: evidence for non-double couple events. Bull Seismol Soc Am 80:88–109

Goertz-Allmann B, Edwards B, Bethmann F, Deichmann N, Clinton J, Fäh D, Giardini D (2011) A new empirical

magnitude scaling relation for Switzerland. Bull Seismol Soc Am 101:3088–3095. https://doi.org/10.1785/0120100291
GRSN (1976) German Regional Seismic Network (GRSN). Federal Institute for Geosciences and Natural Resources (BGR). https://doi.org/10.25928/mbx6-hr74
Grünthal G, Wahlström R (2003) An M_W based earthquake catalogue for central, northern and northwestern Europe using a hierarchy of magnitude conversions. J Seismol 7:507–531
Grünthal G, Wahlström R, Stromeyer D (2009) The unified catalogue of earthquakes in central, northern, and northwestern Europe (CENEC) – updated and expanded to the last millennium. J Seismol 13:517–541
Gutenberg B, Richter CF (1956) Magnitude and energy of earthquakes. Ann Geofis 9:1–15
Hackl M, Malservisi R, Wdowinski S (2009) Strain rate patterns from dense GPS networks. Nat Hazards Earth Syst Sci 9: 1177–1187 www.nat-hazards-earth-syst-sci.net/9/1177/2009/
Hanks TC, Boore DM (1984) Moment-magnitude relations in theory and practice. J Geophys Res 89:6229–6235
Hanks TC, Kanamori H (1979) A moment magnitude scale. J Geophys Res 84:2348–2350. https://doi.org/10.1029/JB084iB05p02348
Haußmann P (1907) Die Erdbebenstation der Technischen Hochchule Aachen. Glückauf Berg- und Hüttenmännische Zeitschrift 26:801–810
Havskov J, Voss PH, Ottemöller L (2020) Seismological observatory software: 30 Yr of SEISAN. Seismol Res Lett 91:1846–1852. https://doi.org/10.1785/0220190313
Hensch M, Dahm T, Ritter JRR, Heimann J, Schmidt B, Stange S, Lehmann K (2019) Deep low-frequency earthquakes reveal ongoing magmatic recharge beneath Laacher See Volcano (Eifel, Germany). Geophys J Int 216:2025–2036. https://doi.org/10.1093/gji/ggy532
Hinzen K-G (1982) Source parameters of mine tremors in the eastern part of the Ruhr district (West Germany). J Geophys 51:105–112
Hinzen K-G (2003) Stress field in the northern Rhine area, Central Europe, from earthquake fault plane solutions. Tectonophysics 377(3–4):325–356
Hinzen K-G (2005) Ground motion parameters of the 22 July 2002 ML 4.9 Alsdorf (Germany) earthquake. Bolletino di Geofisica 46:303–318
Hinzen K-G (2011) Im Erdbebengebiet Rhein-Maas. In: Kraus TR (edt.), Aachen von den Anfängen bis zur Gegenwart, Bd. 1: die natürlichen Grundlagen. - Von der Vorgeschichte bis zu den Karolingern, hrsg. für die Stadt Aachen und den Aachener Geschichtsverein e. V. (Veröffentlichungen des Stadtarchivs Aachen, Bd. 13, zugleich Beihefte der Zeitschrift des Aachener Geschichtsvereins, Bd. 7), Aachen, 57-85
Hinzen K-G (2014) Subway induced vibrations in Cologne Cathedral. Seismol Res Lett 85:631–638
Hinzen K-G (2019) Engineering seismological parameters of two ML 4.3 intraplate earthquakes in the Northern Rhine Area, Germany. Seismol Res Lett 90:1258–1267. https://doi.org/10.1785/0220180265
Hinzen K-G, Fleischer C (2007) A strong motion network in the lower Rhine embayment (SeFoNiB), Germany. Seismol Res Lett 78:502–511
Hinzen K-G, Pietsch S (2000) A seismologically motivated survey of blasting activity in the Northern Rhine Area. Netherlands Journal of Geosciences - Geologie En Mijnbouw 79:73–80. https://doi.org/10.1017/S0016774600021582
Hinzen K-G, Reamer SK (2007) Seismicity, seismotectonics, and seismic hazard in the Northern Rhine Area. In: Stein S, Mazzotti S (edts.) Continental Intraplate Earthquakes: Science, Hazard, and Policy Issues. Geological Society of America Special Paper 425:225–242
Hinzen K-G, Fleischer C, Schock-Werner B, Schweppe G (2012) Seismic surveillance of Cologne Cathedral. Seismol Res Lett 83:9–22
Hutton LK, Boore DM (1987) The ML scale in Southern California. Bull Seismol Soc Am 77:2074–2094
KNMI (1993) Netherlands seismic and acoustic network. Royal Netherlands Meteorological Institute (KNMI). https://doi.org/10.21944/e970fd34-23b9-3411-b366-e4f72877d2c5
Kreemer C, Blewitt G, Davis PM (2020) Geodetic evidence for a buoyant mantle plume beneath the Eifel volcanic area, NW Europe. Geophys J Int 222:1316–1332. https://doi.org/10.1093/gji/ggaa227
LIAG (2020) Schwerekarte der Bundesrepublik Deutschland – Bouguer Anomalien. https://www.leibniz-liag.de/forschung/methoden/gravimetrie-magnetik/bouguer-anomalien.html. Accessed 02 July 2020
Meissner R, Bortfeld R (eds) (1990) DEKORP atlas. Springer, Heidelberg
Meyer W (2013) Geologie der Eifel. Schweizerbart, Stuttgart
Michael AJ (1984) Determination of stress from slip data: faults and folds. J Geophys Res 89:11,517–11,526
Mintrop L (1909a) Die Erdbebenstation der Westfälischen Berggewerkschaftskasse in Bochum, Teil 1/2. Glückauf 45: 357–366
Mintrop L (1909b) Die Erdbebenstation der Westfälischen Berggewerkschaftskasse in Bochum, Teil 2/2. Glückauf 45: 393–403
Munafò I, Malagnini L, Chiaraluce L (2016) On the relationship between M_W and ML for small earthquakes. Bull Seismol Soc Am 106:2402–2408. https://doi.org/10.1785/0120160130
Reamer SK, Hinzen K-G (2004) An earthquake catalog for the Northern Rhine Area, Central Europe (1975-2002). Seismol Res Lett 74:575–582
Ritter J.R.R. (2007). The seismic signature of the Eifel plume. In: Ritter J R R, Christensen U (edts) Mantle plumes: a multidisciplinary approach. Springer, Heidelberg, pp. 379–404
Ritter JRR, Jordan M, Christensen UR, Achauer U (2001) A mantle plume below the Eifel volcanic fields, Germany. Earth Planet Sci Lett 186:7–14
Romanowicz B, Mitchell B (2007) Deep earth structure: Q of the earth from crust to core. https://doi.org/10.1016/B978-0-444-53802-4.00021-X
RUB Germany (2007) RuhrNet - Seismic Network of the Ruhr-University Bochum [Data set]. Federal Institute for Geosciences and Natural Resources. BGR, Germany. https://doi.org/10.7914/SN/RN
Scherbaum F, Hinzen K-G, Ohrnberger M (2003) Determination of shallow shear wave velocity profiles in the Cologne/Germany area using ambient vibrations. Geophys J Int 152: 597–612
Schmincke HU (2007) The quaternary volcanic field of the east and West Eifel (Germany). In: Ritter J R R, Christensen U

(edts) Mantle plumes: a multidisciplinary approach. Springer, Heidelberg, pp. 241–322

Schmincke HU (2009) Vulkane der Eifel. Springer Spektrum, ISBN 978- 3-8274-2367-2

Schwarzbach M (1963) Climates of the past: an introduction to paleoclimatology / Klima der Vorzeit. Van Nostrand, London, xii:328 pp

Sigaran-Loria C, Slob S (2019) Seismic swarms in south Limburg (the Netherlands): tectonic or induced as coal mining lagging effect? VII International Conference on Earthquake Geotechnical Engineering, At Rome, Italy

Snissaert M (1992) PC-based seismic stations, 3 years of experience. Cahiers du Centre Européen de Géodynamique et de Séismologie 5:43–56

University of Cologne (2016) Bensberg earthquake network [data set]. International Federation of Digital Seismograph Networks. https://doi.org/10.7914/SN/BQ

Waldhauser F (2001) hypoDD – a program to compute double-difference hypocenter locations. Technical report, U.S. Geol. Survey, Menlo Park, CA

Zitzmann A (2003) Die Geologische Übersichtskarte 1 : 200 000 – von der Karte bis zur Sachdatenbank. Z Dtsch Geol Ges, 154: 121–139

Zolitschka B, Brauer A, Negendank JFW, Stockhausen H, Lang A, Lottermoser BG (2000) Annually dated late Weichselian continental paleoclimate record from the Eifel, Germany. Geology 28:783–786